AIAA SciTech Forum
7-11 January 2019, San Diego, California
AIAA Scitech 2019 Forum

10.2514/6.2019-0597

Check for updates

Computational Study of a Small Rotor at Hover Using CFD and UVLM

Andrés Pérez G.*, Omar Lopez.†
Universidad de los Andes, Bogotá, 111711, Colombia

Svetlana V. Poroseva‡
University of New Mexico, Albuquerque, New Mexico, 87131, USA

Jaime A. Escobar§
ADVECTOR, Chia, 250002, Colombia

Performance of small rotors is a subject of interest due to increased use of Unmanned Aerial Vehicles (UAVs). In the present paper, numerical simulations of a small rotor commonly used in quadcopters were performed in hover flight. Computational Fluid Dynamics (CFD) and Unsteady Vortex Lattice Method (UVLM) were used and compared. CFD simulations were conducted with the commercial software Fluent ANSYS v17 using the Multiple Reference Frame (MRF) model. In UVLM, a model based on a viscosity dependent growth of the core of the tip vortex was used to account for viscous effects. The wake structure, pressure coefficient distribution on the rotor surface, thrust and torque coefficients obtained by different methods are compared in the paper. Results from flight tests are used to validate thrust and torque predictions. The difference in the prediction of the thrust coefficient between the computational methods is less than 9%. Both methods overestimate the thrust by 3% and 12% for CFD and UVLM respectively with respect to the flight test results.

I. Nomenclature

A	=	Rotor disk Area
G	=	Vortex loop
T	=	Thrust
Q	=	Torque
R	=	Rotor Radius
V_{tip}	=	Tip Velocity
C_p	=	Pressure coefficient
C_T	=	Thrust coefficient
r_c	=	Vortex core radius
Γ	=	Vortex circulation
ρ	=	Density
Ω	=	Angular velocity
δ	=	Turbulent viscosity coefficient
ν	=	Kinematic viscosity
ζ	=	Wake age

*PhD Student, Mechanical Engineering Department, Universidad de los Andes, Bogotá, Colombia, am.perez259@uniandes.edu.co
†Associate Professor, Mechanical Engineering Department, Universidad de los Andes, Bogotá, Colombia, od.lopez20@uniandes.edu.co, AIAA Member.
‡Associate Professor, UNM Mechanical Engineering, 1 University of New Mexico, Albuquerque, NM, poroseva@unm.edu, AIAA Associate Fellow.
§Research and development, ADVECTOR, Chia, Colombia, jaime.escobar@advector.co.

Copyright © 2019 by Andrés Pérez G.
and Omar Lopez and Svetlana V. Poroseva and Jaime A. Escobar. Published by the American Institute of Aeronautics and Astronautics, Inc., with permission.

Downloaded by Suad Jakirlic on January 10, 2019 | http://arc.aiaa.org | DOI: 10.2514/6.2019-0597

II. Introduction

In the last years, Unmanned Aerial Vehicles (UAVs) started to gain more attention from the research community, due to their increased use by various industries such as, for example, agriculture and oil & gas industry, among many others. Quadcopters are the most popular UAV type, because of their rapid takeoff, maneuverability, and easy flight control.

Evaluation of the quadcopter rotor aerodynamic performance is not an easy task though, because of the complexity of the flow field developed by the rotor blades. Preliminary estimates can be obtained using momentum and blade element theories. However, they may not be accurate enough for practical applications, as the theories rely on strong flow simplifications and semi-empirical parameters. Therefore, flow simulations are conducted whenever possible to improve the accuracy of predictions.

Computational Fluid Dynamics (CFD) is the most popular approach to study small rotors aerodynamic performance. Bohorquez (2003) [1] studied the aerodynamic performance of a three-bladed rotor with a diameter of 17.2 cm using CFD simulations. Two alternative rotors were considered: one with untwisted blades and the other with the blades linearly twisted at -10 deg. Both rotors had a root cutout of 16% and an identical rectangular planform with a chord of 1 cm. Each rotor was tested at collective pitch angles ranging from 0 deg to 18 deg in steps of 3 deg. The computational simulations were performed with OVERFLOW-D, using structured overset meshes with a total of 12.6 million grid points. The one-equation Baldwin-Barth turbulence model was used. CFD results had a good qualitative correlation with experiments. However, the thrust coefficient (C_T) was over-predicted by a fairly constant amount. The pressure coefficient C_P was under-predicted at lower collective pitch angles and over-predicted at the higher angles. The maximum predicted figure of merit was almost 20% higher than the one obtained from experimental results.

Lakshminarayan et al (2006) [2] used two overset structured mesh system and the Reynolds-Averaged Navier-Stokes (RANS) solver OVERTURNS to investigate the aerodynamics of a micro hovering rotor, with the Spalart-Allmaras turbulence model [3]. A two-bladed hovering rotor in a flow with with the Reynolds number of 51200, and the Mach number of 0.114, was simulated at different collective angles. At higher collective angles, faster downstream wake convection was observed. The predicted thrust coefficient was in a good agreement with the experimental results, while the figure of merit and the power coefficient (C_P) showed larger differences when compared to experimental data.

Jianhua (2009) [4] developed a new numerical method to simulate the aerodynamic performance of propellers at low Reynolds number using the Baldwin-Lomax algebraic turbulence model [5]. Their grid consisted of two grids: the blade grid and the background grid. In order to reduce the computational cost, RANS equations were solved on the blade grid and the Euler equations were solved on the background grid. Only one of the propeller blades was used in simulations. The influence of other blades was accounted for by using periodic boundary conditions. Simulations results for the propeller efficiency and for the thrust and power coefficients were in agreement with the experimental data.

Hwang et al (2015) [6] conducted flow simulations for hovering and flying forward quadcopters with multiple rotors. They used an unstructured overset-mesh technique and the Spalart-Allmaras turbulence model. In hover, interaction between rotors was found to be weak. In contrast, in forward flight, interaction of the rotors was found to cause the total thrust reduction and the induced periodic variations of the thrust in time. Differences in the thrust values generated by individual rotors were negligible. The resultant moments on the vehicle were small.

Lazaro and Poroseva (2015) [7] studied the effect of the number of blades on the flow structures and the performance of a ducted propeller. CFD simulations were conducted using Menter's Shear Stress Transport version of the $\kappa - \omega$ turbulence model [8] implemented in the commercial CFD software Star-CCM+. Structured and unstructured meshes along with an adaptive mesh refinement for regions with higher vorticity were used in simulations.Blades were untwisted, but fixed at the angle of 10 deg. It was found that the duct contributed up to 30 % in the generated thrust. However, when comparing ducted and unducted propellers with the same number of blades, it was found that unducted propellers had higher thrust coefficient and the figure of merit. That is, more blades should be used in a ducted propeller for its performance to be comparable with that of an unducted one.

Liu (2017) [9] also conducted CFD simulations of small-scale propellers using the Spalart-Allmaras turbulence model. A sliding mesh technique was implemented to simulate the blade rotation. The considered propeller was NR640 with the diameter of 9 in. Simulations were performed for hover and forward flight conditions. The difference between the numerical results for thrust and power coefficients and the experimental data was less than 3%.

Yoon et al (2017) [10] performed high-fidelity computational simulations of two commercial quadcopters with the OVERFLOW solver with the focus on the rotor-fuselage and rotor-rotor aerodynamic interactions. The Detached Eddy Simulation (DES) model based on the Spalart-Allmaras turbulence model was used to simulate isolated rotors and a simplified version of the complete vehicle. A grid was generated for each isolated rotor with a hub and two rotor blades. The mesh for the complete vehicle was constructed by combining grids for isolated rotors. The resulting near-body grids for four rotors and the fuselage consisted of 74 overset grids. A flow around an isolated rotor was simulated for wide

Downloaded by Suad Jakirlic on January 10, 2019 | http://arc.aiaa.org | DOI: 10.2514/6.2019-0597

ranges of angular velocities and collective pitch angles. Comparison of computational results with experimental data showed excellent agreement for the thrust and power coefficients. Numerical results also showed a linear growth of the thrust with the pitch angle and a quadratic behavior for the torque. For the complete vehicle simulation, three different configurations were studied: overmount, undermount, and off-body undermount rotors. It was found that the total thrust generated by the overmount configuration including 4 rotors was 5.1% less than the thrust generated by 4 isolated rotors.

High cost of CFD simulations limits studies on the aerodynamic performance of quadcopters. Therefore, alternative computational techniques are sought for design purposes. Among such techniques are free wake methods that can simulate the wake structure and also predict forces and moments in a good agreement with experimental data [11]. One of such methods is the Unsteady Vortex lattice Method (UVLM), which solves the unsteady potential flow around a lifting surface. This method is used in our study.

Previously, free-vortex wake methods were employed in Shreyas (2006) [11] to study the flow structure around a helicopter rotor during maneuvering flight conditions using. It was observed that the blade tip vortices had a tendency to pair up and bundle into a toroidal ring structure below the rotor. Then, they became unstable and and broke down when convected downstream. Comparisons of the calculated thrust, blade flapping, and the inflow response with available experimental data showed excellent agreement.

Colmenares et al (2015) [12] used the UVLM to simulate a flow around two large rotors with rectangular untwisted blades mounted on a fuselage. The in-house code GUAVLAM was used in simulations of a potential flow around a rotational lifting surface. Simulations were performed with 2, 3, and 4 blades per rotor for 8 revolutions. It was found that interaction of blades with the fuselage caused oscillations of the aerodynamic loads, but the amplitude of these oscillations decreased as the number of blades increased. Numerical results showed that the thrust was strongly influenced by the number of blades and by the geometrical configuration of the two rotors. Aerodynamic loads obtained from the simulations were in a good agreement with experimental data.

To the best of our knowledge, the UVLM has not been previously applied to study a flow around small rotors such as those used in quadcopters. This is the purpose of the current study. Simulations at hover are conducted using the GUAVLAM code. The code is modified to incorporate a viscous correction. A rotor of the quadcopter ARAKNOS V2 from the Colombian company ADVECTOR [13] is used as a prototype. CFD simulations were also performed using ANSYS FLUENT V17. Results from UVLM and CFD simulations are compared and validated against experimental results of flight tests.

Downloaded by Suad Jakirlic on January 10, 2019 | http://arc.aiaa.org | DOI: 10.2514/6.2019-0597

III. Computational Methods

A. Unsteady Vortex Lattice Method

The UVLM [14] is commonly used to simulate an unsteady potential flow around thin lifting surfaces. These surfaces are discretized using rectangular elements called lattices or panels, with a vortex ring being located within every element. As shown in figure 1, a vortex ring is composed of four straight segments of vorticity called vortex filaments. Each vortex ring has a circulation of magnitude G_i and each vortex filament, between panels i and j, has a circulation of magnitude ${\Gamma_i}^j$. In order to enforce the spatial conservation of circulation, G_i is constant for each vortex ring such that the circulation of a vortex filament ${\Gamma_i}^j$ that is at the boundary of two adjacent vortex rings is computed as ${\Gamma_i}^j = G_i - G_j$. A control point (P_i) is defined at the geometrical center of the panel and a normal vector ($\hat{n}_i$) is calculated at this point.

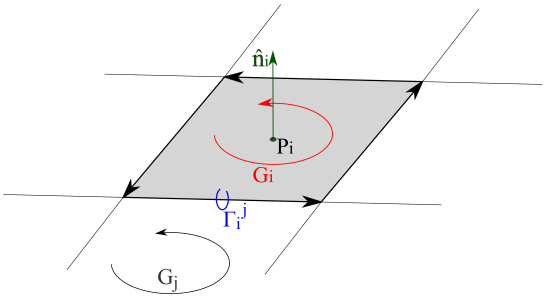

Fig. 1 Vortex ring representation.

The lifting surface is represented by a bound vortex sheet (Fig. 2). When vortex rings in the bound vortex sheet move with the imposed angular velocity Ω, those of them located at the trailing edge are tangentially shed from the lifting surface into a flow [15] forming a wake or a free vortex sheet (Fig. 2). The magnitude of the shed vortex ring circulation remains constant in the process to satisfy Helmholtz's theorem. .

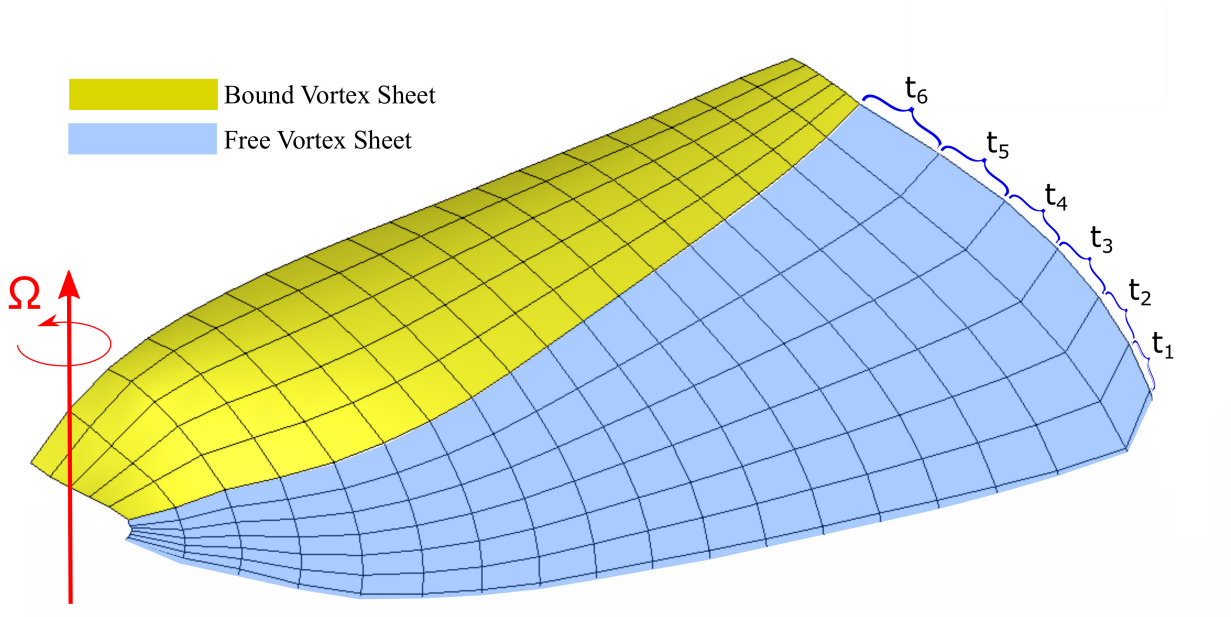

Fig. 2 UVLM wake generation

The circulation of vortex rings at the bound vortex sheet is estimated every time step by imposing the no-penetration boundary condition. This boundary condition is enforced at all control points of the bound vortex sheet. In order to compute the induced velocity of every vortex filament at a control point P_i, the Biot-Savart law:

$$\mathbf{v} = \frac{\Gamma_i{}^j}{4\pi|\mathbf{h}|}\left(\frac{\mathbf{L}\cdot\mathbf{r_1}}{|\mathbf{L}||\mathbf{r_1}|} - \frac{\mathbf{L}\cdot\mathbf{r_2}}{|\mathbf{L}||\mathbf{r_2}|}\right)\frac{\mathbf{L}\times\mathbf{r_1}}{|\mathbf{L}\times\mathbf{r_1}|}, \tag{1}$$

is applied. Figure 3 shows geometrical parameters used in Eq. 1. In the figure, $\mathbf{V}$ is a velocity at the point P_i induced by the vortex filament AB with the circulation $\Gamma_i{}^j$

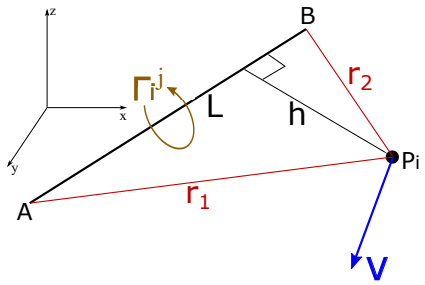

Fig. 3 A velocity induced by the vorticity filament AB.

A linear system of equations

$$\sum_{j=1}^{NBV} a_{i,j}G_j = (\mathbf{V_{Ls,i}} - \mathbf{V_{W,i}} - \mathbf{V}_\infty)\cdot\hat{\mathbf{n}}_\mathbf{i} \tag{2}$$

is obtained when the contribution of all vortex filaments in the bound and free vortex sheets is taken into account. Here, $a_{i,j}$ is the normal component of velocity induced on the panel i by the panel j with the unitary circulation, NBV

Downloaded by Suad Jakirlic on January 10, 2019 | http://arc.aiaa.org | DOI: 10.2514/6.2019-0597

is the number of vortex sheets of the lifting surface, $\mathbf{V_{LS,i}}$ is velocity of the surface at each control point P_i, $\mathbf{V_{W,i}}$ is velocity induced by the free vortex sheet on P_i, and $\mathbf{V}_\infty$ is the free-stream velocity. The vortex filaments of the wake are convected by the free stream velocity and by the velocities induced by the bound and free vortex sheets.

The pressure distribution on the lifting surface is calculated using the unsteady Bernoulli equation. The thrust and the torque generated by the lifting surface can be estimated once the pressure distribution is known.

In the study, UVLM is implemented in the in-house code GUAVLAM [12], which calculates the wake convection using the first-order explicit Euler method. The code is modified for the purposes of the current study by incorporating a predictor-corrector method and a viscous correction.

1. The Predictor-Corrector Method for the Wake Convection

The predictor-corrector scheme is used to improve the Euler method stability. At the predictor step, the Euler explicit method is applied to get an intermediate position for the vortex filaments:

$$\overline{\mathbf{r_{t+1}}} = \mathbf{r_t} + \mathbf{V}(\mathbf{r_t})\Delta t. \tag{3}$$

At the corrector step, the velocity field is estimated from the intermediate positions of the vortex filaments. The new velocity field is used to update the final positions of the vortex rings in the wake:

$$\mathbf{r_{t+1}} = \mathbf{r_t} + \mathbf{V}(\overline{\mathbf{r_{t+1}}})\Delta t. \tag{4}$$

2. Viscous Correction

To avoid singularities in the Biot-Savart law, GUAVLAM uses the Varistas model with $n = 2$ [16]:

$$\mathbf{v} = \frac{\Gamma}{4\pi}\left(\frac{|\mathbf{h}|}{(r_c^4 + |\mathbf{h}|^{\mathbf{4}})^{\frac{1}{2}}}\right)\left(\frac{\mathbf{L}\cdot\mathbf{r_1}}{|\mathbf{L}||\mathbf{r_1}|} - \frac{\mathbf{L}\cdot\mathbf{r_2}}{|\mathbf{L}||\mathbf{r_2}|}\right)\frac{\mathbf{L}\times\mathbf{r_1}}{|\mathbf{L}\times\mathbf{r_1}|}, \tag{5}$$

where r_c is the vortex core radius, which is typically constant. In GUAVLAM, its value is specified to be 5% to 10% of the chord length at the blade tip [17].

In the current study, the value of r_c is modified using a viscous diffusion model:

$$r_c = \sqrt{4\alpha\nu t}, \tag{6}$$

developed from experimental studies [18].In the equation, $\alpha = 1.25643$ is taken from the Lamb-Oseen vortex model for the swirl velocity ([18], [17]).

In the simulations, equation 6 is only used to compute the vortex filaments located at the tip of the bound and free vortex sheets. This is because experimental measurements of the tip vortex core growth [17] showed a higher growth rate than calculated from 6 due to the turbulence vorticity diffusion. To account for this effect,vortex filaments at other locations are calculated using the vortex core radius computed as

$$r_c = \sqrt{4\alpha\delta\nu\frac{\zeta + \zeta_0}{\Omega}} = \sqrt{{r_{c0}}^2 + \frac{4\alpha\delta\nu\zeta}{\Omega}}, \tag{7}$$

where δ is an average "turbulent" viscosity coefficient, $\zeta = \Omega t$ is the wake age (the advanced azimuth angle), and r_{c0} is the vortex core radius at $\zeta = 0$, equal to 5% to 10% of the chord length at the blade tip. The average turbulent viscosity coefficient is a function of the vortex Reynolds number defined as $Re_V = \Gamma/\nu$, where Γ is the circulation of a vortex filament at the tip of the bound and free vortex sheets [17]:

$$\delta = 1 + a_1 Re_V. \tag{8}$$

Here, $a_1 \quad O(10^{-4})$ for small-scale rotors. The value of $a_1 = 2 \times 10^{-4}$ was proposed in [17], and is used in this study.

In the study, simulations are performed using a rotor design described in section IV. The lifting surface in the simulations is the middle surface between the upper and lower surfaces of the rotor blade. To initiate simulations, a slow-starting method is used [12], where the initial value of the non-dimensional angular velocity is close to 0. Then, it is increased up to one in 40 linear steps. After the slow start, the simulations are ran until the thrust coefficient reaches a steady value. The UVLM simulations were executed at the University of New Mexico at a personal computer with $IntelCorei7$ CPU at $3.4GHz$ using 8 cores and with 16GB of memory RAM, the simulation took 5.5 hours.

Downloaded by Suad Jakirlic on January 10, 2019 | http://arc.aiaa.org | DOI: 10.2514/6.2019-0597

B. CFD

CFD simulations were conducted using commercial CFD software ANSYS FLUENT v17.0. Steady-state simulations were performed using the Multi Reference Frame (MRF) model [19] and assuming an incompressible flow. The working fluid was air, with $\rho = 0.877 kg/m^3$ and $\nu = 1.856 \times 10^{-5} kg/m - s$ corresponding to the experimental flow conditions. The air viscosity was calculated using the Sutherland's equation with $T = 24°C$ [20].

1. CFD Computational Domain, mesh and boundary conditions

The object of study is a commercial Carbon fiber rotor $14'' \times 5.5''$ manufactured by RCtimer. A 3D NextEngine Scanner with an accuracy of 0.05mm, was used to digitize the actual rotor and to obtain its CAD model. The rotor has a diameter (DP) of $356mm$, the blade root chord of $20.77mm$, and the blade tip chord of $4.33mm$ as well as the chord length of $25.31mm$ at 75% of the blade span.

The computational domain is a cylinder, with the $3.3DP$ in diameter and $7DP$ in length. As shown in Fig. 4, the center of the rotor is located in the axis of the cylinder at $2.7DP$ from the domain upper surface.

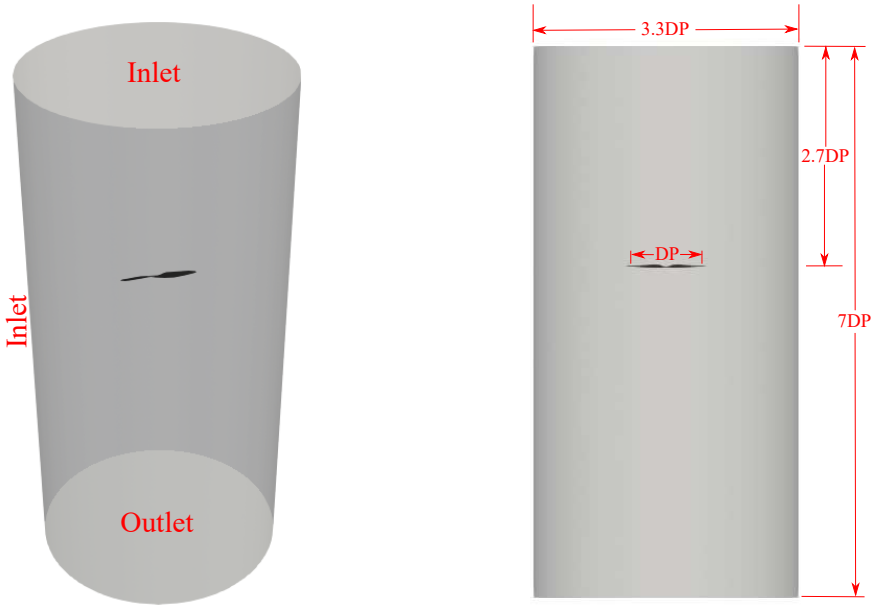

(a) Isometric view

(b) Lateral view

Fig. 4 Computational Domain for CFD Simulations

An unstructured grid of tetrahedral elements is used in the simulations, with a refined layer of pyramidal elements being applied near the rotor surface (Fig. 5). Table 1 provides parameters for five different meshes used in the grid convergence analysis. All the meshes were generated using the ANSYS meshing tool.

Table 1 Mesh Characteristics for the Convergence Study.

Mesh	Size	Refinement Height	Number of Layers	Growth Rate	Average Wall Y+
A	831828	*Without*	*Without*	*Without*	1.22
B	2490082	$1cm$	20	1.2	0.32
C	3280026	$1cm$	20	1.2	0.33
D	5108935	$2cm$	35	1.2	0.33
E	9268866	$2cm$	35	1.2	0.33

Boundary conditions were set as the pressure inlet for the upper and lateral surfaces of the domain and the pressure

Downloaded by Suad Jakirlic on January 10, 2019 | http://arc.aiaa.org | DOI: 10.2514/6.2019-0597

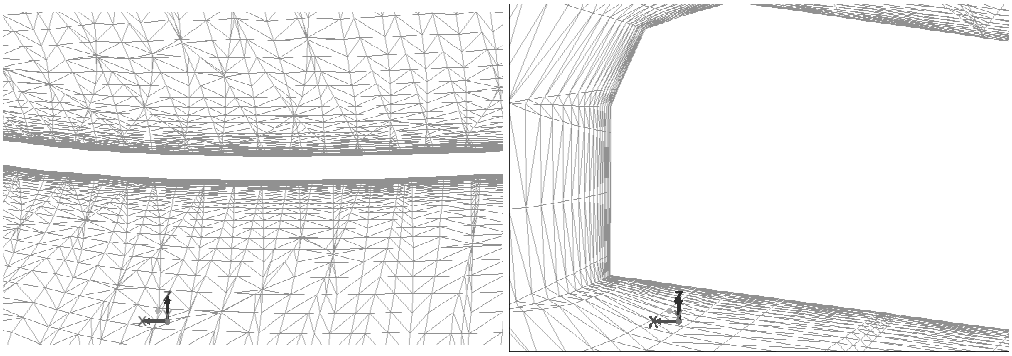

(a) General Mesh Around the Blade **(b) Detail of the Mesh at the Blade Tip**

Fig. 5 Mesh

Downloaded by Suad Jakirlic on January 10, 2019 | http://arc.aiaa.org | DOI: 10.2514/6.2019-0597

outlet for the lower face of the cylinder. The magnitude of the gauge pressure at the boundaries was set equal to 0, but the reference pressure (used to compute the pressure coefficients) was set equal to the atmospheric pressure measured during the experimental tests. This specification of the boundary conditions allows the solver to compute the air flow entrainment from the upper part of the domain and also the induced velocity of the rotor.

2. Solver configuration

The Semi-Implicit Method for Pressure Linked Equations (SIMPLE) is used as a pressure-velocity coupling scheme. The second-order upwind discretization is applied to the convective terms in all the equations. The flow is assumed to be fully turbulent. The shear stress transport SST $k-\omega$ model [8] is employed to model turbulence. The inlet boundary conditions for turbulence are assumed as 5% in the turbulence intensity, as this variable was not measured during the experimental flight tests.

In the simulations, the angular velocity is discretely increased from $1RPM$ up to $4500RPM$. The maximum Reynolds number based on the chord length at 75% of the blade span is 1.1×10^5. Each discrete step approximately doubles the previous velocity. The simulation convergence criterion for each angular velocity was set to 1×10^{-6}. Complete simulations (from 1 RPM up to 4500RPM) took approximately 90000 iterations, and the total CPU time required was approximately 10 days. The simulations were performed with 32 parallel processes using INTEL XEON E5-2695 v2 processors.

IV. Experimental Methodology

A total of nine flight test were performed using the quadcopter ARAKNOS V2 of the Colombian company ADVECTOR (figure 6) [13]. The standard empty weight of the quadcopter was $17.825N$ (including the supplier battery weight). The payload weight used in all tests was $8.39N$, which was achieved by placing battery packs at the bottom of the quadcopter.

The quadcopter uses four $14'' \times 5.5''$ carbon fiber rotors, fixed directly to the motors. Each motor is a brushless Rctimer 5010-530KV with the maximum power of 230.9 W at 14.8 V. The distance between rotors is 620 mm. More detail about the ARAKNOS V2 quadcopter can be found in [21].

The flight test were conducted in Bogotá, Colombia at the altitude of 2640 m.a.s.l. Each test was a three-minutes hover flight at $15m$ above the ground. All tests were performed in an open field, sequentially on the same day, and using new charged batteries between the tests.

The Davis Vantage Pro 2 meteorological station was used to measure the atmospheric pressure and temperature during the flights. The atmospheric pressure was $748hPa$, and the average temperature was $24°C$. The RPM-PWM correlation for the motors was measured at the ground with a strobe light tachometer Monarch.

Flights were monitored using the software 'Mission Planner' [22], which provided real-time information about the battery voltage and currents to the motors. The flight data was collected by an inertial measurement unit (IMU), barometer, and a voltage/current sensor installed on the quadcopter. The voltage and current outputs were recorded by the autopilot and downloaded to a PC for analysis. The barometer data and data for the current and the voltage

were collected and post-processed during the quadcopter takeoff, climb, hover, and descent. However, they were only analyzed for hover. The angular velocity during hover was held to an approximately constant value.

The axperimental thrust measurement at $4500RPM$ was $6.55N$. This corresponds to the experimental thrust coefficient of $C_T = 1.068 \times 10^{-2}$. Since the torque of the motor cannot be measured directly during a flight test, its value was estimated using data for the current, the angular velocity, and the motor efficiency.

Fig. 6 Araknos V2

V. Results

Numerical results are organized as follows. First, an analysis of the effects of the number of panels and the time step on the UVLM simulation results is presented. After that, results of the mesh convergence study for CFD simulations are provided. Then, numerical results of the CFD and UVLM simulations are shown and compared with each other. Simulation results are also validated against experimental results..

A. Influence of the number of panels and time step

For UVLM, a numerical study was conducted to determine effects of the number of panels and the time step on the thrust coefficient. The number of panels varied from 15 to 55 along the blade span and from 5 to 10 along the blade chord as shown in Table 2. Other numerical parameters such as time step (equivalent to a 10° rotation of a blade), angular velocity of $4500RPM$, number of revolutions, initial core radius, and slow start iterations were held constant for this study. The effect on the prediction of C_T was found to be insignificant, that is, less than 1% in considered three cases (Table 2). On the other hand, the computational time increased more than the order of magnitude comparing the cases with the minimum and maximum panels.

Table 2 Number of panels effect on the UVLM results

Divisions	Panels	C_T	Simulation Time
15×5	75	1.136×10^{-2}	$842s$
33×7	231	1.149×10^{-2}	$3887s$
55×10	550	1.143×10^{-2}	$11037s$

To analyze the time step effect, simulations were conducted using three different time steps (equivalent to a certain number of degrees of the blade rotation): 5°, 10°, and 15° (Table 3). In these simulations, the number of panels was constant: 33×7. The effect on the thrust coefficient was again found to be insignificant as the table data demonstrate, but the computational time varied substantially.

Based on the results presented in Tables 2 and 3, all the following UVLM simulations were obtained using the 33×7 number of panels and the time step equivalent to the rotation angle of 10° at the angular velocity of $4500RPM$.

Downloaded by Suad Jakirlic on January 10, 2019 | http://arc.aiaa.org | DOI: 10.2514/6.2019-0597

Table 3 Time discretization effects on the UVLM results

Time Step	C_T	Simulation Time
15°	1.141×10^{-2}	$1544s$
10°	1.149×10^{-2}	$3887s$
5°	1.146×10^{-2}	$22464s$

B. The Grid Convergence Analysis for CFD simulations

The mesh convergence analysis was performed using 6 different meshes with the total number of elements varying from 0.8 to 16.5 million cells. Values of the thrust and torque coefficients at the angular velocity of $5221RPM$ were chosen as the convergence criteria. This velocity value was chosen based on the preliminary flight tests, and approximately corresponds to the medium velocity within the range of the operational velocities of the quadcopter.

Figure 7 shows predicted values of the two coefficients obtained when using different meshes. The thrust and torque coefficients vary less than 0.2% and 0.03%, respectively, when the number of elements is increased from 9.6 to 16.5 million. Therefore, the mesh with 9.6 million cells was chosen to conduct following CFD simulations. The value of the angular velocity is $4500RPM$ in all simulations.

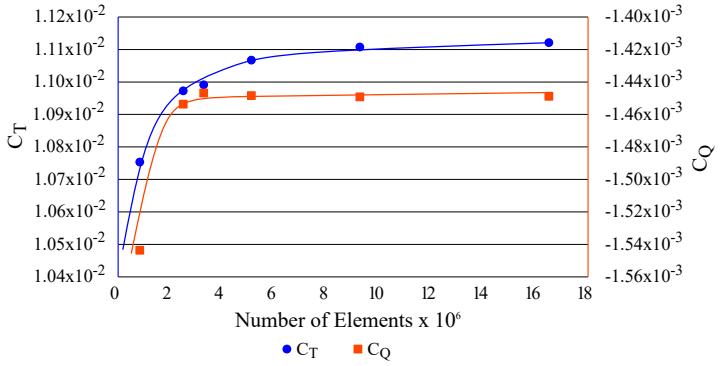

Fig. 7 Variations of the thrust and moment with the number of the mesh cells

C. Wake

Figure 8 shows the wake predicted by CFD and UVLM simulations. The wake obtained in the CFD simulations is visualized using the Q-criterion (see ref. [23]), while the wake from the UVLM simulations is visualized as the free vortex sheets shed into a flow. The CFD results show a steady-state wake visualized from the reference frame attached to the rotor, whereas the wake from the UVLM simulations is instantaneous recorded at the last time step.

Although different, both simulation methods show a strong vortex structure at the tip of the blade and a helical path followed by the descending tip and inner vortices in agreement with the theoretical wake descriptions [18] [24].

The descent angle of the tip vortex is approximated from figure 9: 5.4° in the CFD simulations and 4.2° in the UVLM simulations. In UVLM, it was observed that the descent angle increased with the distance to the rotor.

D. Pressure Coefficient

Predictions of the C_p distribution along the rotor obtained from the CFD and UVLM simulations are shown in figure 10. Some similarity between the CFD and UVLM results can be observed in the coefficient distribution, but the high pressure area is larger in the UVLM simulations. This may be a consequence of the low number of panels used in these simulations in comparison with the fine surface mesh used in the CFD simulations.

Downloaded by Suad Jakirlic on January 10, 2019 | http://arc.aiaa.org | DOI: 10.2514/6.2019-0597

Downloaded by Suad Jakirlic on January 10, 2019 | http://arc.aiaa.org | DOI: 10.2514/6.2019-0597

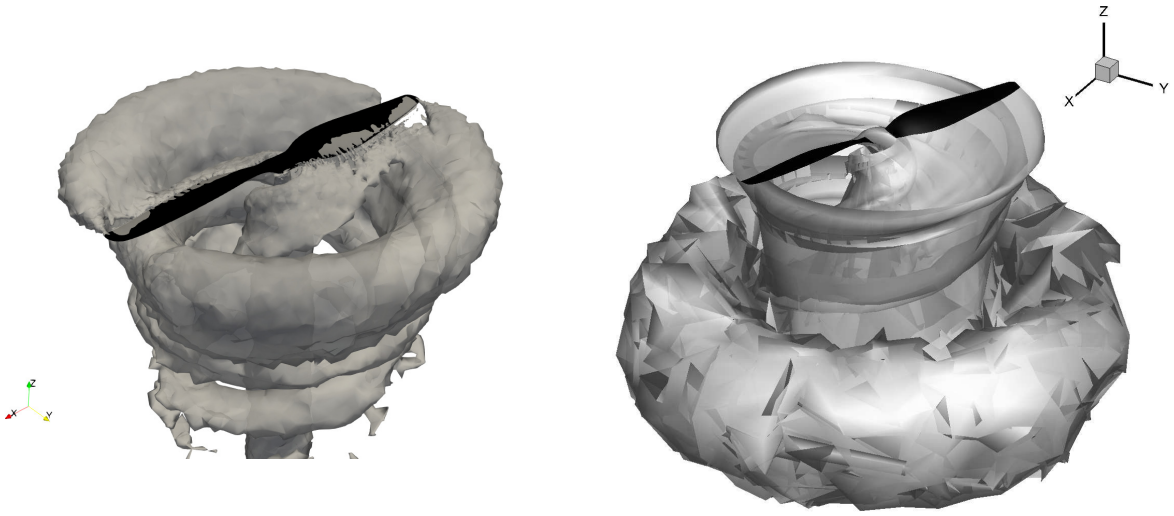

(a) CFD Wake, Q-Criterion

(b) UVLM Wake, Vortex Sheets

Fig. 8 Wake Visualization

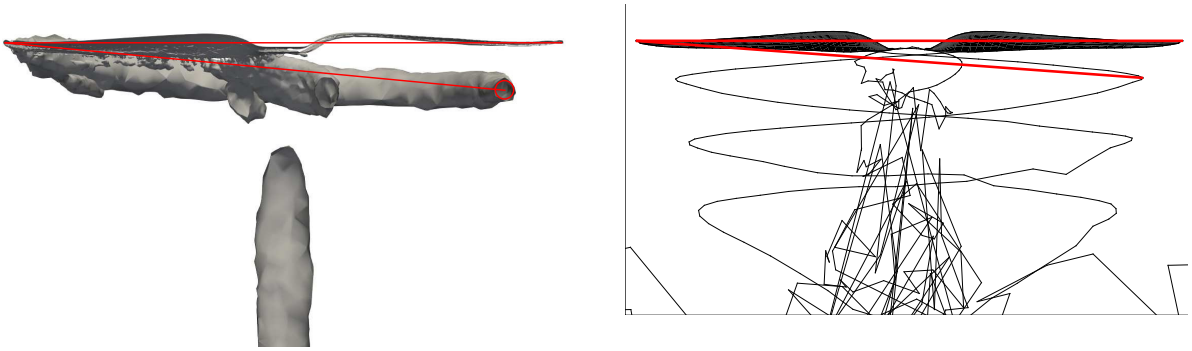

(a) CFD Wake Angle, Q-Criterion

(b) UVLM Wake Angle, Vortex Sheets

Fig. 9 Angle of Descend of the Tip Vortex for $\zeta = 180°$

E. Thrust Coefficient

Figure 11 shows evolution of the thrust coefficient in time obtained from the UVLM simulations. The simulations ran for 328 time steps to ensure that C_T reaches a steady value. The final value, $C_T = 1.1959 \times 10^{-2}$, is calculated as the average during the last revolution at $4500RPM$. TO calculate C_T fron CFD simulations, the definition of thrust coefficient 9 was applied [18]

$$C_T = \frac{T}{\rho A {V_{tip}}^2} \tag{9}$$

The value obtained is $C_T = 1.1045 \times 10^{-2}$ at 4500 RPM. The difference in the predictions obtained with the two methods is less than 9%. Table 4 provides comparison of the computed values of the thrust coefficient with the experimental data. Both methods overestimate the generated thrust by 3% for CFD and 12% for UVLM simulations.

(a) CFD C_p

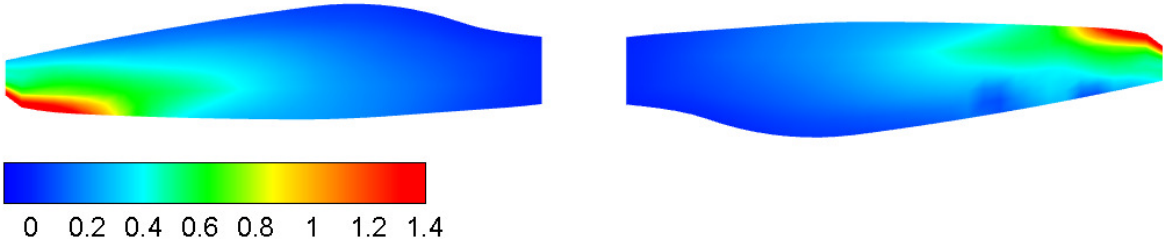

(b) UVLM C_p

Fig. 10 Rotor Pressure Coefficient Distribution

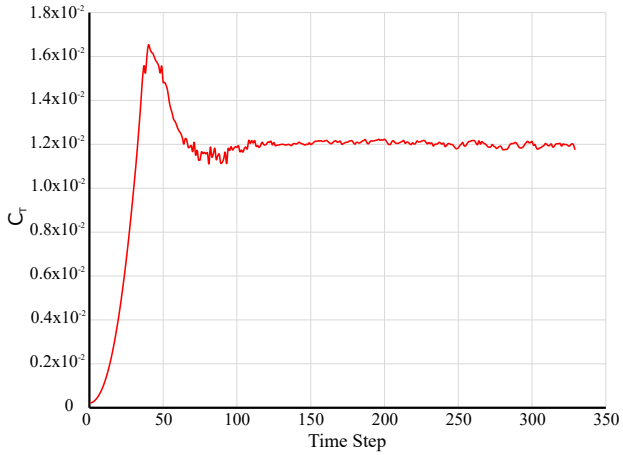

Fig. 11 Thrust Coefficient from UVLM

Table 4 Thrust Comparison vs. Experimental

	Experimental	*CFD*	*UVLM*
Thrust Coefficient	1.068×10^{-2}	1.1045×10^{-2}	1.1959×10^{-2}
Difference vs Experimental		3.34%	11.89%

F. Torque Coefficient

Figure 12 shows the torque coefficient as a function of time obtained from the UVLM simulations. The average magnitude of the torque coefficient is $C_Q = 1.1769 \times 10^{-3}$, while in the CFD simulations, it is $C_Q = 1.4307 \times 10^{-3}$. The torque coefficients were calculated as [18].

Downloaded by Suad Jakirlic on January 10, 2019 | http://arc.aiaa.org | DOI: 10.2514/6.2019-0597

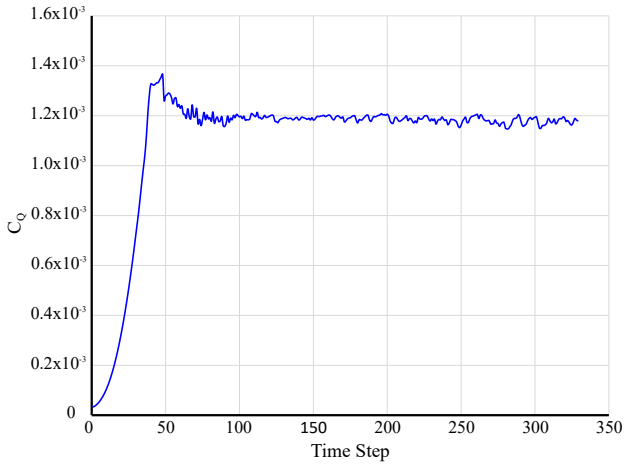

Fig. 12 Torque Coefficient from UVLM

$$C_Q = \frac{Q}{\rho A {V_{tip}}^2 R} \tag{10}$$

The difference between the predicted torque coefficients is 17%. Table 5 compares computed torque coefficients with the experimental data. The CFD simulations overpredicts the torque coefficient by 15%, while the UVLM simulations underpredict this parameter by 4%..

Table 5 Torque Comparison vs. Experimental

	Experimental	*CFD*	*UVLM*
Torque Coefficient	1.2356×10^{-3}	1.4307×10^{-3}	1.1769×10^{-3}
Difference vs Experimental		15.79%	−4.75%

VI. Conclusions

Results of simulations of the flow around a small rotor flying in hover using two different computational methods (UVLM and CFD) were shown and discussed. Despite the differences in the formulation of the two computational methods numerical results were in fairly good agreement with experimental data based on flight test. Specifically, the UVLM provides a complete visualization of the wake directly as result of the unsteady convection of vorticity from the blade to the wake. In CFD simulations, it is is necessary to apply a vortex visualization method based on Q criteria to study the wake structure. However, both methods predict a similar wake structure and descent angle of the tip vortex. The predictions of the contours of pressure coefficient along the blade are similar for both methods i.e. same value range is observed. A difference of approximately 9% in the thrust coefficient prediction was obtained between CFD and UVLM. For UVLM, prediction of the torque coefficient was 11% higher when compared to experimental data; while CFD over-predicts this value only by a 3%. Regarding the torque coefficient, CFD overestimated it by a 15%, but in UVLM simulations, the torque was underestimated by 4% .

Overall, UVLM with the proposed viscous correction produces results close to those from CFD simulations and experiments. Thus, this method is a suitable tool to study aerodynamics of small rotors. Moreover, the computational cost of UVLM is much less than that of CFD simulations, making this approach affordable alternative to CFD.

Acknowledgments

The authors would like to thank the 'Departamento Administrativo de Ciencia, Tecnología e Innovación' (COLCIENCIAS) and its program to sponsor Ph.D. students in Colombia; also, the Department of Mechanical Engineering, University of New Mexico, in U.S.A. where the first author spent a year working on the project. Computations

Downloaded by Suad Jakirlic on January 10, 2019 | http://arc.aiaa.org | DOI: 10.2514/6.2019-0597

were conducted using high-performance facilities at Universidad de los Andes and the Center for Advanced Research Computing at the University of New Mexico. We would alos like to express our gratitude to Ms. Laura Juliana Suárez Collazos for her valuable contribution in this investigation.

References

[1] Bohorquez, F., Rankins, F., Baeder, J. D., and Pines, D. J., "Hover Performance of Rotor Blades at Low Reynolds Numbers for Rotary Wing Micro Air Vehicles. An Experimental and CFD Study," *21st Applied Aerodynamics Conference*, 2003.

[2] Lakshminarayan, V. K., Bush, B. L., Duraisamy, K., and Baeder, J. D., "Computational Investigation of Micro Hovering Rotor," *24th Applied Aerodynamics Conference, 5 - 8 June 2006, San Francisco, California*, 2006.

[3] Spalart, P., and Allmaras, S., "A one-equation turbulence model for aerodynamic flows," *American Institute of Aeronautics and Astronautics, Technical Report AIAA-92-0439*, 1992.

[4] Jianhua, X., Wenping, S., and Zhonghua, H., "Calculation of Aerodynamic Performance of Propellers at Low Reynolds Number Based on Reynolds-Averaged Navier-Stokes Equations Simulation," *Computational Fluid Dynamics 2008. Springer, Berlin, Heidelberg*, 2009.

[5] Baldwin, B. S., and Lomax, H., "Thin Layer Approximation and Algebraic Model for Separated Turbulent Flows," *16th Aerospace Sciences Meeting Huntsville, AL, U.S.A*, 1978.

[6] Hwang, J., Jung, M., and Kwon, o., "Numerical Study of Aerodynamic Performance of a Multirotor Unmanned-Aerial-Vehicle Configuration," *Journal of Aircraft*, 2015.

[7] Lazaro, C., and Poroseva, S., "Computational Analysis of the Blade Number Effect on the Performance of a Ducted Propeller," *AIAA Atmospheric Flight Mechanics Conference*, 2015.

[8] Menter, F. R., "Two-equation eddy-viscosity turbulence models for engineering applications," *AIAA Journal*, 1994.

[9] Liu, J., and Luo, S.-B., "Navier-Stokes Equation based Flow Simulations of Low Reynolds Number Propeller for Unmanned Aerial Vehicle," *55th AIAA Aerospace Sciences Meeting*, 2017.

[10] Yoon, S., Diaz, P. V., Boyd, D., Chan, W. M., and Theodore, C. R., "Computational Aerodynamic Modeling of Small Quadcopter Vehicles," *AHS Forum 73*, 2017.

[11] Shreyas, A., "Analysis of Rotor Wake Aerodynamics During Maneuvering Flight Using a Free-Vortex Wake Methodology," Ph.D. thesis, University of Maryland, 2006.

[12] Colmenares, J., López, O., and Preidikman, S., "Computational Study of a Transverse Rotor Aircraft in Hover Using the Unsteady Vortex Lattice Method," *Mathematical Problems in Engineering*, 2015.

[13] Advector, *Advector Unmanned Systems*, http://www.advector.co/, 2014.

[14] Konstadinopoulos, P., Thrasher, D. R., Mook, D. T., Nayfeh, A. H., and Watson, L., "A Vortex-Lattice Method for General, Unsteady Aerodynamics," *Journal of Aircraft, Vol. 22*, 1985.

[15] Preidikman, S., "Numerical Simulations of Interactions among Aerodynamics, Structural Dynamics, and Control Systems." *PhD thesis, Virginia Polytechnic Institute and State University*, 1998.

[16] Vatistas, G., Kozel, V., and Mih, W., "A Simpler Model for Concentrated Vortices," *Experiments in Fluids*, 1991.

[17] Bhagwat, M., and Leishman, G., "Generalized Viscous Vortex Model for Application to Free-Vortex Wake and Aeroacoustic Calculations," 2002.

[18] Leishman, G., *Principles of Helicopter Aerodynamics*, Cambridge University Press, 2008.

[19] Luo, J., Issa, R., and Gosman, A., "Prediction of impeller-induced flows in mixing vessels using multiple frames of referenc." *In IChemE Symposium Series*, 1994.

[20] Crane, C., *Flow of Fluids Through Valves, Fittings, and Pipe*, Crane Co, 1982.

[21] Advector, *ARAKNOS V2 specs*, http://www.advector.co/en/products.htmlAraknos, 2014.

[22] Team, A. D., *Mission Planner Home*, http://ardupilot.org/planner/, 2016.

Downloaded by Suad Jakirlic on January 10, 2019 | http://arc.aiaa.org | DOI: 10.2514/6.2019-0597

[23] Holmen, V., "Methods for vortex identification," Master's thesis, Mathematics (Faculty of Technology) and Numerical Analysis. Lund University, 2012.

[24] Seddon, J., *Basic Helicopter Aerodynamics*, BSP Professional Books, 1990.

Downloaded by Suad Jakirlic on January 10, 2019 | http://arc.aiaa.org | DOI: 10.2514/6.2019-0597